Surface-Mounted Tilt Sensor Using Fiber Bragg Grating Technology for Engineered Slope Monitoring With Temperature Compensation

M. S. M. Sa'ad, H. Ahmad, M. A. Alias, M. K. A. Zaini, K. S. Lim, *Senior Member, IEEE*, S. W. Harun, K. T. V. Grattan, B. M. A. Rahman, *Life Fellow, IEEE*, G. Brambilla, S. A. Reduan, L. Bayang, and M. F. Ismail

***Abstract*—A surface-mounted tilt sensor was designed and fabricated to measure the inclination angle of engineered structures or slopes in two directions. The device utilizes two strain-sensitive fiber Bragg gratings (FBGs) for tilt angle measurement bidirectionally and one strain-free FBG to provide temperature compensation. In this work, a tilt sensor prototype was fabricated using a 3-D printer, with a robust enclosure and a miniature actuator with dimensions of 115 × 65 × 30 mm and 45 × 20 × 3 mm, respectively. The device was first calibrated in the laboratory for tilt and temperature parameters. For tilt calibration, the device yields a sensitivity value of 0.0135 and 0.0123 nm/° for +*x*- and −*x*-directions. On the other hand, the device delivers a sensitivity value of 0.0105 nm/°C as the response to temperature changes. The tilt sensor was also tested for suitability in a real-field deployment where it was installed on a retaining wall and was left for four weeks. The field test data indicate no vertical displacement of the wall since the device exhibits zero inclination changes during the test period. This compact, robust, and easy-to-install tilt sensor has excellent potential for various geotechnical applications, mainly in landslide detections, ground movement, and engineered slope monitoring.**

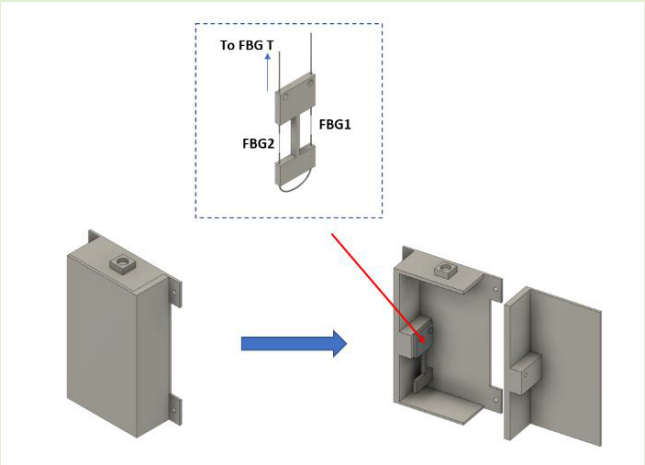

***Index Terms*— Engineered slope monitoring, fiber Bragg gratings (FBGs), ground movement, landslides, tilt sensor.**

I. Introduction

A LANDSLIDE is a mass movement of rock, soil, or debris down a slope due to gravitational pull [1]. This catastrophic event could occur on natural and engineered slopes with different magnitudes and velocities. Hence, it is crucial to identify the extent and speed of a ground movement to provide a reliable predictive analysis for the landslide early warning system. Fundamentally, tilt sensors measure angular deviations of a plane with respect to another reference plane. This type of sensor can be found in numerous applications in various sectors. For example, in geotechnical areas, tilt sensors or tiltmeters are often found on buildings and bridges to monitor these structures for structural stress and vertical deformation that may occur due to extensive ground movement [2], [3]. In addition, tilt sensors are typically installed or directly attached to landslide mitigation structures, such as retaining walls, to monitor high-risk slopes for landslides that could occur due to many reasons, such as earthquakes, heavy rainfall, and human activities [4], [5], [6].

Conventional electrical-based tilt sensors are typically based on either magnetic [7] or capacitive effects [8]. Although these sensors possess high sensitivity and accuracy, they are susceptible to short circuits, which could be caused by water or liquid mixtures in environments with high humidity levels. There are also low-voltage displays based on

Manuscript received 13 April 2023; accepted 14 April 2023. Date of publication 25 April 2023; date of current version 14 June 2023. This work was supported in part by the Universiti Malaya under Grant UM-Innovate PPSI-2020-HICOE-02 and in part by the British Council-MIGHT Newton Ungku Omar Fund (NUOF) under Grant IF022-2020. The work of K. T. V. Grattan was supported by the Royal Academy of Engineering. The associate editor coordinating the review of this article and approving it for publication was Prof. Carlos Marques. *(Corresponding author: H. Ahmad.)*

M. S. M. Sa'ad, M. A. Alias, M. K. A. Zaini, K. S. Lim, S. A. Reduan, L. Bayang, and M. F. Ismail are with the Photonics Research Center, Universiti Malaya, Kuala Lumpur 50603, Malaysia.

H. Ahmad is with the Photonics Research Center and the Physics Department, Faculty of Science, Universiti Malaya, Kuala Lumpur 50603, Malaysia, and also with the Universiti Kuala Lumpur British Malaysian Institute (UniKL BMI), 53100 Selangor, Malaysia (e-mail: harith@um.edu.my).

S. W. Harun is with the Department of Electrical Engineering, Faculty of Engineering, Universiti Malaya, Kuala Lumpur 50603, Malaysia.

K. T. V. Grattan and B. M. A. Rahman are with the School of Mathematics, Computer Science and Engineering, City, University of London, EC1V 0HB London, U.K.

G. Brambilla is with the Optoelectronics Research Centre, University of Southampton, SO17 1BJ Southampton, U.K.

complementary metal-oxide semiconductor (CMOS) technology that could be implemented as sensors' display; however, the device still depends on electrical power [9], [10]. Besides that, electrical-based sensors are prone to lightning strikes and are easily affected by electromagnetic interference, a common problem faced by end users in field applications. These are the main reasons why optical-based sensors are preferred nowadays over electrical-based sensors in ground movement monitoring and landslide detection. Furthermore, unlike electrical-based sensors, optical sensors are immune to electromagnetic interference, short circuit, and thunder strikes, making them suitable for implementation in harsh environments.

Various optical fiber-based sensors have been proposed in the past in geotechnical sectors and structural health monitoring, such as Michelson interferometer sensors [11], Fabry–Perot strain sensors [12], Brillouin's scatter-based distributed sensors [13], [14], and fiber Bragg grating (FBG) sensors [15], [16], [17], [18], [19], [20], [21], [22], [23], [24], [25], [26], [27], [28]. FBG-based sensors are among the best options due to their multiplexing capabilities and the utilization of long fiber optics cables, which are crucial in monitoring high-risk slopes remotely [29]. Since FBGs have been introduced for sensing applications, numerous types of FBG-based sensors have been developed for various engineering applications.

In the past decade, research focused on implementing FBG-based sensors in geotechnical applications has grown exponentially [18], [24], [28], [30], [31], [32], [33], [34], [35]. For example, Ni et al. [18] successfully determined the inclination of a circular base plate by hanging weight to the base plate using four FBGs, similar to the pendulum structure. The authors calibrated their sensors from $-10°$ to $10°$ of tilt and within 5 °C–45 °C of temperature. However, such bulky and rotation-sensitive design is considered unsuitable for field deployment, especially in geotechnical applications. In another work, a technique based on a pendulum was proposed by Xu et al. [35], but in their case, the sensor came with a rigid shaft in the middle directly attached to a dead weight. Furthermore, they utilized only two FBGs for single-axis tilt measurements and calibrated their sensor only from $-3°$ to $3°$ of the tilting angles without discussing the temperature compensation method.

Table I shows a comparison between the proposed sensor and previous works on FBG-based tilt sensors. During the past five years, there were three reports that were presented in the development of FBG-based tilt sensors using the 3-D printing technology. Although several devices possess better sensitivity values, their design is bulky and comprises complex mechanical parts, which render their sensor unsuitable for field applications. There are no reports regarding the implementation of such tilt sensors in real-field applications [19], [20], [24] except in this demonstration.

Furthermore, although several lab-scale validations had been conducted, to the best of our knowledge, there were no explicit explanations provided regarding the temperature compensation method on raw wavelength data from real-field applications [20], [23], [24], [25], [26], [27], [28], [42].

TABLE I
TABLE OF COMPARISON BETWEEN EXISTING LITERATURE AND THE PROPOSED SENSOR

Ref	Year	No of FBG	Range (°)	Sensitivity (nm/°)	Temperature compensation method	3D printing technology	Tested for real field application
H.J. Chen et al [36]	2008	1	15	0.06	Mechanical	No	No
M. Liang et al [37]	2019	3	±30°	0.03	Strain-free FBG	No	No
C.Y. Hong et al [24]	2019	2	±75°	0.01	Wavelength ratio difference	Yes	Miniaturized lab-scale model
Y. Guo et al [38]	2020	2	±90°	0.02	Wavelength ratio difference	No	No
K. Li et al [39]	2020	2	±50°	0.001	-	No	No
N. Ismail et al [20]	2021	4	±90°	0.01	Strain-free FBG	Yes	No
N. Ismail et al [19]	2021	4	±90°	0.01	Strain-free FBG	Yes	No
A. Gautam [40]	2022	1	±4°	0.1	-	No	No
Y. Guo et al [41]	2023	2	±15°	0.1	Wavelength ratio difference	No	No
This work	2023	3	±45°	0.013	Strain-free FBG	Yes	Yes

This article presents a surface-mounted tilt sensor utilizing two strain-sensitive FBGs for tilt measurement and one strain-free FBG to provide a temperature compensation factor. The tilt sensor prototype was fabricated using a 3-D printer using polylactic acid (PLA) and thermoplastic polyurethane (TPU) as its primary printing material. The device had been calibrated inside the laboratory, and to obtain real-field application data, it was later tested on a retaining wall of an engineered slope. Furthermore, the field data were processed to display the final measurement output by compensating the wavelength shift value of the strain-free FBG, which was further discussed in Section III.

II. METHODOLOGY

This section comprises five subsections. Section II-A describes the fabrication of FBG used in this work, while Section II-B highlights the actuator design, which was fabricated by using a 3-D printer. Then, Section II-C presents the enclosure design, which houses the actuator, followed by Section II-D, which is the calibration procedure inside the laboratory. Finally, Section II-E details the field test procedures in which the sensor was installed on a retaining wall in the campus.

A. Fabrication of FBG

All the FBGs used in this work were inscribed by exposing the core of a standard single-mode fiber (SMF-28) to a strong pulse of ultraviolet (UV) light using the phase mask method. Before the inscription process can be conducted, the SMF must be hydrogen loaded by soaking the SMF in a hydrogen-filled tube for seven days at room temperature to photosensitize the fiber. This process ensured that the fiber was more reactive toward the UV light. In addition, the photochemical interaction between dissolved H_2 molecules and UV laser caused significant electron excitations, which quickens the grating formation [43]. Shortly, after the fiber was removed from the hydrogen-filled tube, light pulses from a 248-nm krypton fluoride (KrF) excimer laser were shined onto the fiber through a phase mask,

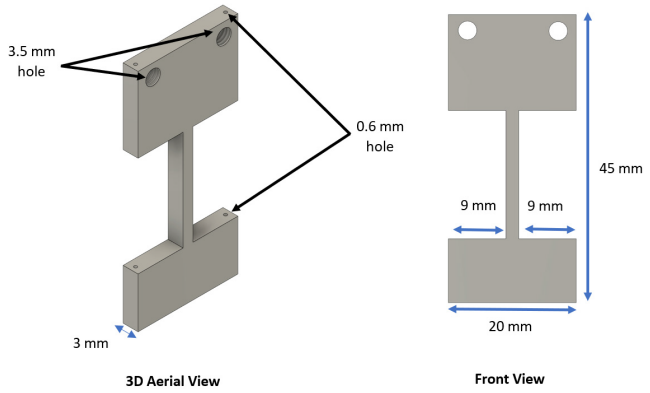

Fig. 1. Actuator design.

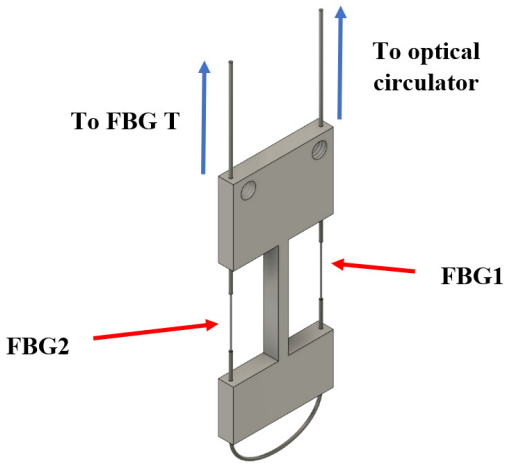

Fig. 2. FBG installation to the actuator.

inscribing a uniform grating into the fiber core. After the inscribing process was completed, the fiber was stored in an oven at 80 °C for 7 h to remove the remaining hydrogen.

For Bragg gratings that were inscribed into a single-mode fiber, the Bragg wavelength λ_B is directly related to strain, ε, and temperature, T, which can be calculated by using the general FBG equation as follows:

$$\frac{\Delta\lambda_B}{\lambda_B} = (1 - p_{\text{eff}})\,\Delta\varepsilon + (\alpha + \xi)\Delta T \tag{1}$$

where $\Delta\lambda_B$ is the change of the Bragg wavelength and p_{eff} is the photoelastic coefficient. Besides that, α and ξ are the thermal expansion and thermo-optic coefficient of the standard SMF, respectively.

B. Actuator Design

The main sensing unit of the device was a 3-D printed actuator that was fabricated by using the material TPU. The actuator was designed to be compact, with a dimension of only 45 × 20 × 3 mm (length × width × thickness). For field deployment, a smaller sensor is preferable since this would ease the installation process and significantly reduce the space occupied by the sensors. This would enable the sensors to be deployed in tight areas, which would provide more opportunities for the sensor to be applied. The actuator was printed by using a 0.4-mm nozzle with 0.1-mm printing resolution. The infill density of the print was set to 100%. Fig. 1 shows the actuator design, which has a 2-mm-thick rectangular shaft in the middle of the structure. A rectangular shaft was used instead of a cylindrical shaft because it has a definite directional movement, eliminating the possibility of rotational twists in the cylindrical shaft. After the printing process, the actuator was left on a table for 1 h at room temperature. This procedure acts as a precaution because if an FBG is fit on a hot actuator, the FBG will gradually loosen as the hot actuator undergoes compression during the cooling process. After an hour of cooling, FBG1 and FBG2 with a reflective peak wavelength of 1537.64 and 1542.75 nm were installed to the actuator through the 0.6 mm holes, opposite to each other, as shown in Fig. 2. Since the loose FBG could give erroneous measurements, a prestrain procedure was conducted. Both ends of the fiber were pulled with a pulling stage before cyanoacrylate glue was used to permanently bond the fiber to the actuator. Then, a strain-free FBGT with a reflective wavelength of 1548.00 nm was spliced together, enabling the device to have three distinct wavelengths in a single output. Since the FBGT is free from strain variation and is not bonded to any structure, it will provide a reliable temperature compensation factor for this device.

C. Enclosure Design

The main motivation behind the enclosure design was to make the sensor deployable in harsh environment. Hence, fragile FBGs need to be protected to avoid damage to the gratings. The enclosure was designed with a dimension of 30 × 65 × 115 mm (length × width × height) and was 3-D printed in two parts using the PLA material. The enclosure was printed in two parts to ease the assembly procedures. The enclosure was also equipped with a fiber adapter socket and four 6.0-mm holes to enable the device to be mounted on flat surfaces. As shown in Fig. 3, the enclosure can be easily opened by removing the front part, allowing the actuator to be fixed to the enclosure's internal fixture using a screw with a diameter of 3.0 mm through the 3.5-mm hole. PLA was chosen because it is relatively cheap compared to other 3-D printing materials and it is resistant to ambient temperatures up to 60 °C–65 °C. However, other enclosure materials, such as acrylonitrile butadiene styrene (ABS) and polycarbonate (PC), could always be used as an alternative to suit installations in various climates and environmental temperatures since they have a higher heat resistance compared to PLA.

D. Device Calibration in the Laboratory

After the device had been fully assembled, both tilting angle and temperature calibration procedures were conducted in the laboratory at a constant room temperature of 25 °C. The main objective of this calibration is to obtain the sensitivity value of the device toward tilt variation, where in this case, nm per degree of tilt (nm/°). This value is crucial in determining the exact tilt, which can be obtained from the wavelength shift of the FBG.

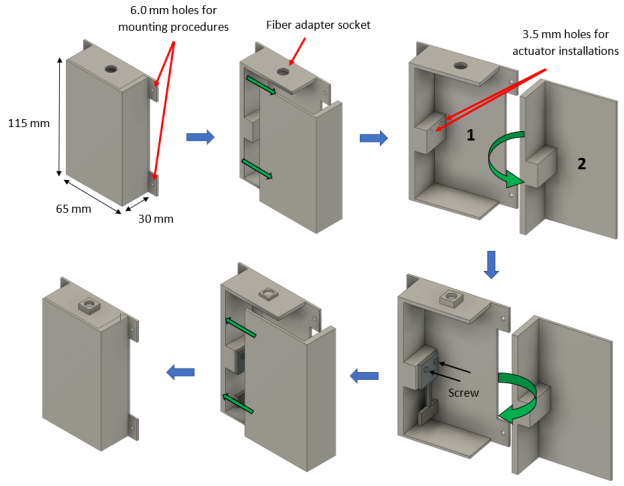

Fig. 3. Surface-mounted tilt sensor assembly procedure.

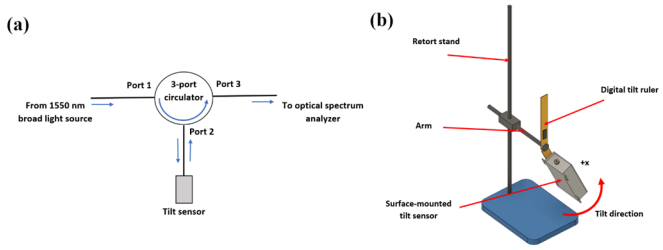

Fig. 4. (a) Schematic of the sensor's interrogation setup and (b) illustration of the tilt calibration procedure.

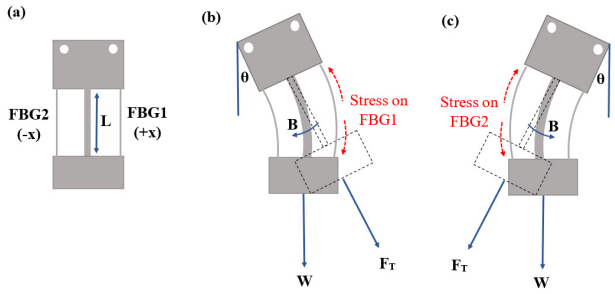

Fig. 5. Illustration of the actuator (a) at the initial position of 0 tilt angle, (b) during the tilt toward the $+x$-direction, and (c) during the tilt toward the $-x$-direction.

1) Tilting Angle Calibration: The schematic of the tilting angle calibration setup is given in Fig. 4(a). The output from the tilt sensor was directly connected to Port 2 of the three-port circulator, where a broad 1550-nm light source was used to illuminate port 1. Port 3 was connected to an optical spectrum analyzer (OSA) with a wavelength resolution of 0.02 nm, where the wavelength spectra were observed and analyzed. The device was vertically mounted to a digital tilt ruler before it was tilted toward the $+x$-direction from 0° to 45° tilt angle, as shown in Fig. 4(b). This procedure was repeated five times to evaluate the measurement accuracy and repeatability of the sensor. Then, the tilt calibration procedure was repeated by tilting the device toward the $-x$-direction.

Fig. 5(a) shows the sensor orientation at 0° tilt angle. At the initial position of 0° tilt angle, both FBG1 and FBG2 are subjected to initial tensional stress due to the weight of the bottom part, W, which is the product of the mass m and the gravitational pull g such that $W = mg$. In Fig. 5(b), when the sensor was tilted toward the $+x$-direction (defined as the bottom part moved toward the $+x$-direction), the fiber facing the $+x$-direction would be stretched due to the tensile force F_T and the bending moment B acting on the middle shaft, causing an increase in the tensional stress onto FBG1. This resulted in the shifts of the FBG1 reflective wavelength to the right. A similar case can be applied for FBG2 when the sensor was tilted toward the $-x$-direction, as shown in Fig. 5(c).

As illustrated in the figure, the tensile force, F_T, and the bending moment, B, of the sensor can be expressed as follows [24]:

$$F_T = W \cos\theta \tag{2}$$

$$B = W.L \sin\theta \tag{3}$$

where W is the weight of the bent structure and L is the bending arm length, which, in this case, is the length of the middle shaft. Since both tensile force F_T and bending moment B would exert strain on the FBGs, the strain exerted on the grating ε can be written as follows:

$$\varepsilon = \frac{F_T}{EA_s} \pm \frac{B}{EI_S} \tag{4}$$

where E, A_s, and I_S are referred to as the elastic modulus, the cross-sectional area of the shaft, and the moment of inertia of the shaft, respectively. Equation (4) can be further simplified to be expressed as follows:

$$\varepsilon = \frac{W}{E}\left(\frac{\cos\theta}{A_s} \pm \frac{L\sin\theta}{I_S}\right). \tag{5}$$

2) Temperature Calibration: The device was then placed inside a water bath, leaving all FBGs fully immersed in the water to ensure that the heat changes were distributed evenly among the FBGs. The water bath temperature increased from 30 °C to 70 °C in 5 °C intervals, while the spectrum plot was taken using an OSA. Then, the device was left inside the water bath for 5 h to analyze the stability of the sensor measurement toward temperature. The measurement was taken hourly by using the same spectrum analyzer.

E. Field Test

After all calibrations in the laboratory had been completed, the surface-mounted tilt sensor was installed on a slope retaining wall that had been affected by some soil movement. The site was chosen because a minor landslide had occurred previously, damaging and moving part of the walls and the nearby road. Upon inspection and initial measurement carried out by the civil engineers of the maintenance department, the affected retaining wall had inclined forward with a value of 9.26°, indicating a need to monitor if there is any significant postevent ground movement. Before the sensor installation, the wall was first ground with a sanding machine to ensure a smooth surface. Next, four 6-mm holes were drilled where the sensor was then vertically fixed to the wall, with the front of the device facing the inclination direction, as shown in Fig. 6.

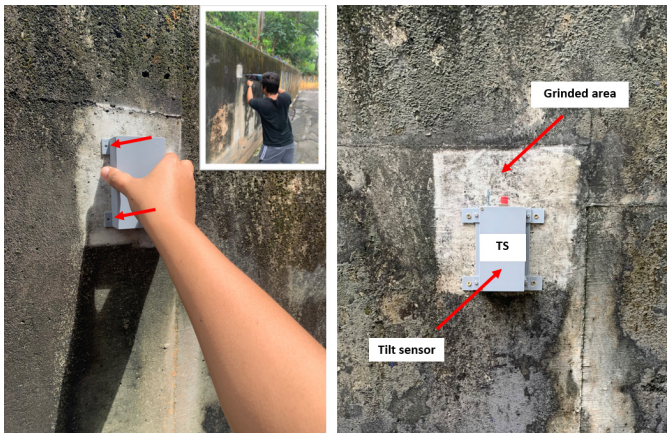

Fig. 6. Installation of the surface-mounted tilt sensor onto the retaining wall.

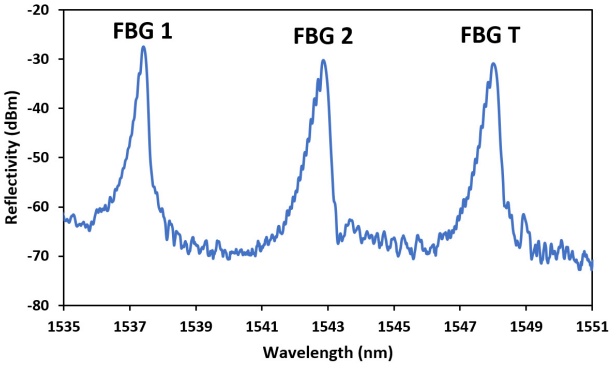

Fig. 7. Initial wavelength spectrum of the device at a 0° of tilt angle shows three reflective peaks of FBG1, FBG2, and FBGT.

The sensor was only allowed to be left for four weeks before reconstruction works took place. The measurement was taken weekly at noon using an FBG interrogator with a resolution of 10 P.M. and 3000-Hz sampling speed.

III. Results and Discussion

This section presents the device calibration and the field deployment test, as given in Sections III-A and III-B, respectively.

A. Device Calibration in the Laboratory Results

1) Tilting Angle Calibration: The initial wavelength spectrum of the device at 0° of tilting angle is given in Fig. 7. As labeled in the figure, three reflective peaks are present from FBG 1, FBG 2, and FBG T, representing the $+x$, $-x$, and temperature compensation.

As the tilt sensor was tilted 45° toward $+x$-direction at 5° intervals, the shifts in the wavelength spectrum of FBG 1 could be observed in Fig. 8(a). On the other hand, when the tilt sensor was tilted 45° toward the $-x$-direction at 5° intervals, a similar shift pattern was observed at FBG 2, as shown in Fig. 8(b). This figure shows that each FBG only shifted when the sensor was tilted toward its respective direction. Furthermore, for both tilt cases, we could observe that FBG T did not exhibit any shift in the wavelength, proving that

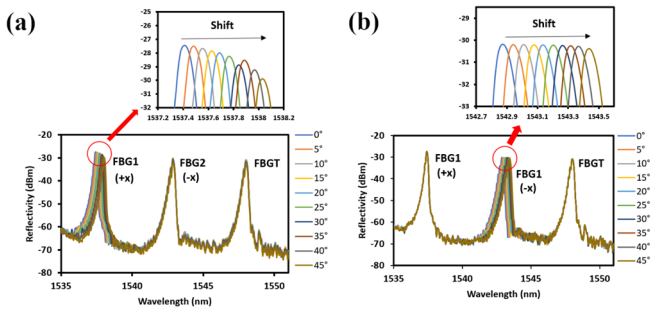

Fig. 8. Wavelength spectra of FBG1, FBG2, and FBT during 0°–45° tilt toward (a) $+x$-direction and (b) $-x$-direction.

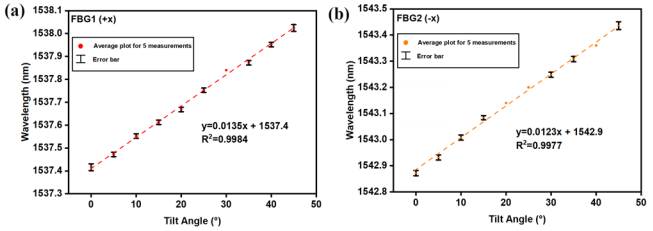

Fig. 9. Linear response with their respective error bars for (a) FBG1 and (b) FBG2 during the tilt calibration of the tilt sensor.

FBG T is indeed strain-free and can provide a temperature compensation factor for the device.

The bandwidth of FBG is directly connected to the grating length. The relationship between these two parameters is inversely proportional in which, by increasing the grating length, FBG with a smaller bandwidth would be obtained. FBG with a smaller bandwidth provides better measurement accuracy compared to those with a larger bandwidth because the peak wavelength can be distinguished more accurately. In sensing applications, although FBG with a smaller bandwidth is preferable to minimize errors in the measurement, this would result in a longer grating length, which would affect the size of the device. A bigger actuator is required to mount the FBG. This would result in difficulties during the installation of the sensor and would not provide a very compact device. Hence, there is a need to balance between the size of the device and its measurement accuracy to achieve the most optimum tilt sensors. In this work, the grating length of the FBG is 1 cm, which provides us with the FBG bandwidth between 0.15 and 0.25 nm with more than 90% reflectivity. This enables a compact device with a sensitivity value of 0.013 nm/° to be fabricated, which has been proven suitable and sufficient for field applications.

The sensitivity of the tilt sensor was determined by plotting the wavelength versus tilt angles, as given in Fig. 9. Fig. 9(a) and (b) shows the linear plot of the device when it was tilted toward the $+x$- and $-x$-direction, respectively. It was determined that the device exhibits a tilt sensitivity value of 0.0135 and 0.0123 nm/° for 0°–45° tilt toward the $+x$- and $-x$-direction, respectively.

These calibration values are crucial in determining the tilt angle of the device during field applications. For instance, when the device is tilted toward the $+x$-direction at an unknown tilt angle X°, the corresponding wavelength shift of

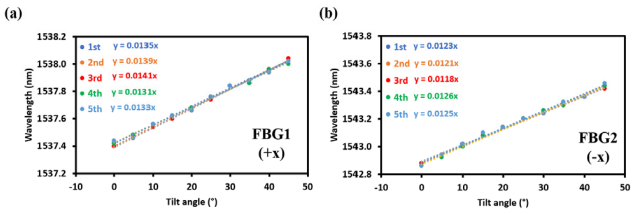

Fig. 10. Wavelength versus tilt angle plot for five sets of tilt calibration measurements for (a) FBG1 and (b) FBG2.

the affected FBG $\Delta\lambda_B$ could be used to calculate the tilt angle by using the following equation:

$$\frac{0.0135\ \text{nm}}{1^\circ} = \frac{\Delta\lambda_B}{X^\circ}. \tag{6}$$

Besides that, from the laboratory calibration results, it was seen that our proposed device recorded a 30% increase in the sensitivity value compared to sensors with PLA-based structures. This was simply because TPU is more elastic when compared to PLA due to its lower Young's modulus value, which makes TPU more flexible as a middle shaft [44], [45]. A middle shaft that was fabricated by using TPU would cause the bottom part of the sensor to exert larger tensional strain on the gratings. This would then lead to a larger wavelength shift with each tilt variation, resulting in a steeper linearity graph with a higher gradient value. This indicates that the sensor has a higher sensitivity value. This statement is supported by (4), which validates that dividing the tensile force and the bend moment with a smaller Young's modulus value would cause a larger strain and vice versa.

Furthermore, Fig. 10 has been plotted to evaluate the accuracy and repeatability of the fabricated sensor. The plot shows that the sensor yields insignificant different sensitivity values since the data were acquired using an OSA with a wavelength resolution of 0.02 nm. Hence, it was safe to assume that the device is highly accurate and repeatable, with an average tilt sensitivity of 0.01 nm/°. Nonetheless, the margin of error was extremely low, with a standard deviation value of 0.0004 and 0.0003 nm for a tilt toward $+x$ and $-x$, respectively.

2) Temperature Calibration: During the temperature calibration, as the water bath temperature was raised from 30 °C to 70 °C, the wavelength shifts could be observed clearly in Fig. 11(a) for FBG1, FBG2, and FBGT. All FBGs shifted to the right since all FBGs were immersed in the water and evenly exposed to significant temperature variations inside the water bath. Fig. 11(b) highlights each FBG response toward temperature changes, with an identical sensitivity value of 0.0105 nm/°C. Similar sensitivity to temperature changes proves that FBGT would provide a reliable temperature compensation factor. This indicates that mounting the FBGs to the 3-D-printed actuator did not impose any unintended stress on the gratings since the FBG was not directly embedded into the TPU, which would have been a different case. The sensor has also shown an excellent temperature stability up to 70 °C, as shown in Fig. 11(c). The wavelength of FBGT was constant at 1548.46 nm during the 5-h test in a 70 °C water bath. This validates that the wavelength measurement of FBGT was indeed stable, making it suitable to be used as the temperature compensation FBG for this device.

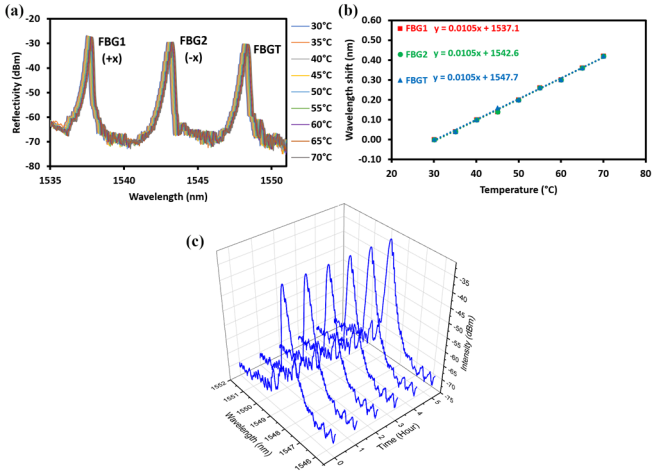

Fig. 11. (a) Wavelength spectrum of the tilt sensor during the temperature calibration process; (b) corresponding linear response for FBG1, FBG2, and FBGT toward temperature changes; and (c) 3-D plot of the FBGT wavelength at 70 °C over the period of 5 h.

TABLE II
INITIAL MEASUREMENT OF THE TILT SENSOR FOR FBG1, FBG2, AND FBGT RIGHT AFTER THE INSTALLATION

Initial measurement (Base reading)	
Sensor	**FBG peak wavelength (corrected to 2 decimal points)**
FBG1 (+x)	1537.99 nm
FBG2 (-x)	1542.97 nm
FBGT	1548.22 nm

B. Field Deployment Test

Table II shows the initial peak wavelength measurement of the device for FBG1, FBG2, and FBGT after the tilt sensor had been installed on the retaining wall. In Table II, the wavelength measurement was tabulated in two sections. First, the data from the interrogator were resolved to two decimal points. Then, after comparing the wavelength shift of each FBG with its reference value during the laboratory calibration, our proposed tilt sensor determined that the wall had inclined forward with an inclination value of 9.63°, which proved that the device was indeed accurate with an error of only 4% from the measurement carried out earlier by the maintenance engineers. Then, the sensor was zeroed, in which the values from Table II were considered the new base measurement at 0° tilt angle.

The sensor measurements on weeks 2–4 were tabulated in Table III. The table has three extra columns: the total wavelength shift, the strain-sensitive wavelength shift, and the inclination of the device. The entire wavelength shift was acquired by subtracting the current wavelength measurement from its respective reference value in Table II. In this peak

TABLE III
DEVICE WAVELENGTH MEASUREMENT ON WEEKS 2–4

Week 2

Sensor	Wavelength (corrected to 2 decimal points)	Total Wavelength Shift (nm)	Wavelength shift only due to strain (nm)	Deviation from initial measurement (°)
FBG1 (+x)	1538.00 nm	0.01	0	0
FBG2 (-x)	1542.98 nm	0.01	0	0
FBGT	1548.23 nm	0.01	-	-

Week 3

Sensor	Wavelength (corrected to 2 decimal points)	Total Wavelength Shift (nm)	Wavelength shift only due to strain (nm)	Deviation from initial measurement (°)
FBG1 (+x)	1538.00 nm	0.01	0	0
FBG2 (-x)	1542.98 nm	0.01	0	0
FBGT	1548.23 nm	0.01	-	-

Week 4

Sensor	Wavelength (corrected to 2 decimal points)	Total Wavelength Shift (nm)	Wavelength shift only due to strain (nm)	Deviation from initial measurement (°)
FBG1 (+x)	1538.00 nm	0.01	0	0
FBG2 (-x)	1542.98 nm	0.01	0	0
FBGT	1548.23 nm	0.01	-	-

wavelength analysis, it is essential to note that FBGs are affected by both strain and temperature. Hence, the total wavelength shifts for FBG1 and FBG2 must be subtracted by the wavelength shift values indicated by the strain-free FBGT to obtain the wavelength shift that is only due to strain.

Furthermore, as mentioned previously, from the tabulated data, the device's inclination could be calculated using (6). As an example, for week 1, FBG1 in Table II recorded a 0-nm wavelength shift that is only due to strain after subtracting its total wavelength shift with FBGT. By inserting these values into (6), the following equation can be derived as follows:

$$\frac{0.0135\ \text{nm}}{1^\circ} = \frac{0\ \text{nm}}{X^\circ}. \tag{7}$$

These data highlight the implementation of the temperature compensation technique in the peak wavelength analysis of FBG-based sensors. All the tabulated data showed that each FBG exhibited a total wavelength shift of 0.01 nm. Since FBGT was a strain-free FBG, this indicates that there were temperature variations that caused all FBG to shift at a similar rate. As mentioned above, the wavelength shifts of FBG1 and FBG2 had been subtracted by the FBGT wavelength shift, indicating a 0-nm shift due to strain, leading to 0° vertical deviation of the device when compared to the initial measurement. This is consistent with the weekly measurement recorded by the maintenance engineer, which also stated that there was no subsequent movement of the wall since the initial measurement was taken.

Another crucial aspect to highlight in this section is the relationship between the resolution of an FBG interrogator and the final output of the measured FBG-based tilt sensor. In our case, since the minimum reliable wavelength shift that the interrogator can detect is only 10 pm, this would make the minimum inclination angle that can be detected is 0.8°. By using a simple Pythagorean theorem, the minimum vertical displacement resolution of a 1-m structure that could be obtained is 0.01 mm/m. It is important to note that an interrogator with a higher wavelength resolution of 1 pm could provide a better vertical displacement resolution of up to 0.001 mm/m, which can match the specifications of a conventional sensor.

IV. CONCLUSION

An FBG-based, surface-mounted tilt sensor has been proposed and fabricated for field applications. In this tilt sensor, an actuator that holds the FBG was attached to a compact, lightweight, and robust enclosure that fully protects the fragile FBG from harsh environments. The field test proved the sensor reliability and is able to withstand harsh environments. Therefore, this device is highly beneficial to the community, especially in the early detection of landslides and structural health monitoring.

REFERENCES

[1] F. C. Dai, C. F. Lee, and Y. Y. Ngai, "Landslide risk assessment and management: An overview," *Eng. Geol.*, vol. 64, no. 1, pp. 65–87, 2002, doi: 10.1016/S0013-7952(01)00093-X.

[2] T. H. T. Chan et al., "Fiber Bragg grating sensors for structural health monitoring of Tsing ma bridge: Background and experimental observation," *Eng. Struct.*, vol. 28, no. 5, pp. 648–659, Apr. 2006, doi: 10.1016/j.engstruct.2005.09.018.

[3] H. F. Lima et al., "Structural health monitoring of the church of Santa Casa da MisericÓrdia of Aveiro using FBG sensors," *IEEE Sensors J.*, vol. 8, no. 7, pp. 1236–1242, Jul. 2008, doi: 10.1109/JSEN.2008.926177.

[4] Y. Yoshida, Y. Kashiwai, E. Murakami, S. Ishida, and N. Hashiguchi, "Development of the monitoring system for slope deformations with fiber Bragg grating arrays," *Proc. SPIE*, vol. 4694, pp. 296–303, Jul. 2002, doi: 10.1117/12.472632.

[5] Y.-T. Ho, A.-B. Huang, J. Ma, and B. Zhang, "Ground movement monitoring using an optic fiber Bragg grating sensored system," in *Proc. 17th Int. Conf. Opt. Fibre Sensors*, vol. 5855, May 2005, p. 1020, doi: 10.1117/12.623596.

[6] C.-Y. Hong, Y.-F. Zhang, M.-X. Zhang, L. M. G. Leung, and L.-Q. Liu, "Application of FBG sensors for geotechnical health monitoring, a review of sensor design, implementation methods and packaging techniques," *Sens. Actuators A, Phys.*, vol. 244, pp. 184–197, Jun. 2016, doi: 10.1016/j.sna.2016.04.033.

[7] R. Olaru and C. Cotae, "Tilt sensor with magnetic liquid," *Sens. Actuators A, Phys.*, vol. 59, nos. 1–3, pp. 133–135, 1997, doi: 10.1016/S0924-4247(97)80162-8.

[8] *Inclinometers: Types, How They Work, & Functions*. Accessed: Jan. 7, 2021. [Online]. Available: https://www.encardio.com/blog/inclinometer-types-how-it-works-uses/

[9] Z. Li, K. Zhu, X. Huang, J. Zhao, and K. Xu, "All silicon microdisplay fabricated utilizing 0.18 μm CMOS-IC with monolithic integration," *IEEE Photon. J.*, vol. 14, no. 2, pp. 1–5, Apr. 2022, doi: 10.1109/JPHOT.2022.3160226.

[10] K. Xu, "Silicon electro-optic micro-modulator fabricated in standard CMOS technology as components for all silicon monolithic integrated optoelectronic systems," *J. Micromech. Microeng.*, vol. 31, no. 5, May 2021, Art. no. 054001, doi: 10.1088/1361-6439/abf333.

[11] L. M. N. Amaral, O. Frazao, J. L. Santos, and A. B. L. Ribeiro, "Fiber-optic inclinometer based on taper Michelson interferometer," *IEEE Sensors J.*, vol. 11, no. 9, pp. 1811–1814, Sep. 2011, doi: 10.1109/JSEN.2011.2105264.

[12] Y. Yang, X. Ma, K. Chen, E. Wang, Z. Yu, and Q. Yu, "A high-resolution dynamic fiber-optic inclinometer," *Sens. Actuators A, Phys.*, vol. 283, pp. 305–312, Nov. 2018, doi: 10.1016/j.sna.2018.10.007.

[13] M. F. Ghazali, H. Mohamad, and K. A. Ang, "Development of distributed fibre optic inclinometer for landslide and geotechnical application," in *Proc. 16th Asian Regional Conf. Soil Mech. Geotechnical Eng.*, 2020, pp. 3–6.

[14] L. Schenato et al., "Distributed optical fibre sensing for early detection of shallow landslides triggering," *Sci. Rep.*, vol. 7, no. 1, pp. 1–7, Oct. 2017, doi: 10.1038/s41598-017-12610-1.

[15] R. Min, B. Ortega, and C. Marques, "Fabrication of tunable chirped mPOF Bragg gratings using a uniform phase mask," *Opt. Exp.*, vol. 26, no. 4, p. 4411, Feb. 2018, doi: 10.1364/oe.26.004411.

[16] C. A. F. Marques et al., "Fast Bragg grating inscription in PMMA polymer optical fibres: Impact of thermal pre-treatment of preforms," *Sensors*, vol. 17, no. 4, pp. 1–8, 2017, doi: 10.3390/s17040891.

[17] Y. L. Wang, B. Shi, T. L. Zhang, H. H. Zhu, Q. Jie, and Q. Sun, "Introduction to an FBG-based inclinometer and its application to landslide monitoring," *J. Civil Struct. Health Monitor.*, vol. 5, no. 5, pp. 645–653, Nov. 2015, doi: 10.1007/s13349-015-0129-4.

[18] K. Ni, X. Dong, Y. Jin, and H. Xu, "Temperature-independent fiber Bragg grating tilt sensor," *Microw. Opt. Technol. Lett.*, vol. 52, no. 10, pp. 2250–2252, Oct. 2010, doi: 10.1002/mop.25425.

[19] N. N. Ismail et al., "Biaxial 3D-printed inclinometer based on fiber Bragg grating technology," *IEEE Sensors J.*, vol. 21, no. 17, pp. 18815–18822, Sep. 2021, doi: 10.1109/JSEN.2021.3090105.

[20] N. N. Ismail et al., "Novel 3D-printed biaxial tilt sensor based on fiber Bragg grating sensing approach," *Sens. Actuators A, Phys.*, vol. 330, Oct. 2021, Art. no. 112864, doi: 10.1016/j.sna.2021.112864.

[21] A. G. Leal-Junior, V. Campos, C. Díaz, R. M. Andrade, A. Frizera, and C. Marques, "A machine learning approach for simultaneous measurement of magnetic field position and intensity with fiber Bragg grating and magnetorheological fluid," *Opt. Fiber Technol.*, vol. 56, May 2020, Art. no. 102184, doi: 10.1016/j.yofte.2020.102184.

[22] M. Ghorat, G. B. Gharehpetian, H. Latifi, M. A. Hejazi, and M. Bagheri, "High-resolution FBG-based fiber-optic sensor with temperature compensation for PD monitoring," *Sensors*, vol. 19, no. 23, pp. 1–14, 2019, doi: 10.3390/s19235285.

[23] M. Maheshwari, Y. Yang, D. Upadrashta, and T. Chaturvedi, "A rotation independent in-place inclinometer/tilt sensor based on fiber Bragg grating," *IEEE Trans. Instrum. Meas.*, vol. 68, no. 8, pp. 2943–2953, Aug. 2019, doi: 10.1109/TIM.2018.2870246.

[24] C. Hong, Y. Zhang, Z. Lu, and Z. Yin, "A FBG tilt sensor fabricated using 3D printing technique for monitoring ground movement," *IEEE Sensors J.*, vol. 19, no. 15, pp. 6392–6399, Aug. 2019, doi: 10.1109/JSEN.2019.2908873.

[25] S. He, X. Dong, K. Ni, Y. Jin, C. C. Chan, and P. Shum, "Temperature-insensitive 2D tilt sensor with three fiber Bragg gratings," *Meas. Sci. Technol.*, vol. 21, no. 2, Feb. 2010, Art. no. 025203, doi: 10.1088/0957-0233/21/2/025203.

[26] H. Y. Au, S. K. Khijwania, H. Y. Fu, W. H. Chung, and H. Y. Tam, "Temperature-insensitive fiber Bragg grating based tilt sensor with large dynamic range," *J. Lightw. Technol.*, vol. 29, no. 11, pp. 1714–1720, Jun. 2011, doi: 10.1109/JLT.2011.2132695.

[27] H. Bao, X. Dong, L.-Y. Shao, C.-L. Zhao, and S. Jin, "Temperature-insensitive 2-D tilt sensor by incorporating fiber Bragg gratings with a hybrid pendulum," *Opt. Commun.*, vol. 283, no. 24, pp. 5021–5024, Dec. 2010, doi: 10.1016/j.optcom.2010.07.050.

[28] X. Dong, L. Hu, L. Shao, Y. Wang, and J. Zheng, "Temperature-insensitive 2D fiber Bragg grating TILT sensor," *Microw. Opt. Technol. Lett.*, vol. 55, no. 2, pp. 344–346, Feb. 2013, doi: 10.1002/mop.27281.

[29] A. D. Kersey et al., "Fiber grating sensors," *J. Lightw. Technol.*, vol. 15, no. 8, pp. 1442–1462, Aug. 15, 1997, doi: 10.1109/50.618377.

[30] T.-C. Liang and Y.-L. Lin, "Ground vibrations detection with fiber optic sensor," *Opt. Commun.*, vol. 285, no. 9, pp. 2363–2367, May 2012, doi: 10.1016/j.optcom.2012.01.037.

[31] H.-F. Pei, J.-H. Yin, H.-H. Zhu, C.-Y. Hong, W. Jin, and D.-S. Xu, "Monitoring of lateral displacements of a slope using a series of special fibre Bragg grating-based in-place inclinometers," *Meas. Sci. Technol.*, vol. 23, no. 2, Feb. 2012, Art. no. 025007, doi: 10.1088/0957-0233/23/2/025007.

[32] A.-B. Huang, J.-T. Lee, Y.-T. Ho, Y.-F. Chiu, and S.-Y. Cheng, "Stability monitoring of rainfall-induced deep landslides through pore pressure profile measurements," *Soils Found.*, vol. 52, no. 4, pp. 737–747, Aug. 2012, doi: 10.1016/j.sandf.2012.07.013.

[33] D. Sengupta, M. S. Shankar, P. S. Reddy, R. L. N. S. Prasad, and K. Srimannarayana, "Sensing of hydrostatic pressure using FBG sensor for liquid level measurement," *Microw. Opt. Technol. Lett.*, vol. 54, no. 7, pp. 1679–1683, Jul. 2012.

[34] H. Pei, J. Yin, and W. Jin, "Development of novel optical fiber sensors for measuring tilts and displacements of geotechnical structures," *Proc. SPIE*, vol. 4694, Jun. 2013, Art. no. 095202, doi: 10.1088/0957-0233/24/9/095202.

[35] H. Xu, F. Li, W. Zhao, S. Wang, Y. Du, and C. Bian, "A high precision fiber Bragg grating inclination sensor for slope monitoring," *J. Sensors*, vol. 2019, pp. 1–7, Jun. 2019, doi: 10.1155/2019/1354029.

[36] H.-J. Chen, L. Wang, and W. F. Liu, "Temperature-insensitive fiber Bragg grating tilt sensor," *Appl. Opt.*, vol. 47, no. 4, pp. 556–560, Jan. 2008, doi: 10.1364/AO.47.000556.

[37] M. Liang, X. Fang, S. Li, G. Wu, M. Ma, and Y. Zhang, "A fiber Bragg grating tilt sensor for posture monitoring of hydraulic supports in coal mine working face," *Measurement*, vol. 138, pp. 305–313, May 2019, doi: 10.1016/j.measurement.2019.02.060.

[38] Y. Guo, C. Li, X. Zhou, L. Jiang, and H. Liu, "Wide-range fiber Bragg grating tilt sensor based on a cam structure," *IEEE Sensors J.*, vol. 20, no. 9, pp. 4740–4748, May 2020, doi: 10.1109/JSEN.2020.2967088.

[39] K. Li, Y. Zhao, Y. Li, G. Liu, and J. Li, "Fiber Bragg grating biaxial tilt sensor using one optical fiber," *Optik*, vol. 218, Sep. 2020, Art. no. 164973, doi: 10.1016/j.ijleo.2020.164973.

[40] A. Gautam and A. Kumar, "Highly sensitive FBG based tilt sensor using PM-IM conversion and EFD interrogation technique," *IEEE Trans. Instrum. Meas.*, vol. 71, pp. 1–9, 2022, doi: 10.1109/TIM.2022.3172430.

[41] Y. Guo, P. Hu, L. Xiong, K. Liu, and W. Zhou, "Design and investigation of a fiber Bragg grating tilt sensor with vibration damping," *IEEE Sensors J.*, vol. 23, no. 3, pp. 2193–2203, Feb. 2023, doi: 10.1109/JSEN.2022.3229397.

[42] X. Dong, C. Zhan, K. Hu, P. Shum, and C. Chiu Chan, "Temperature-insensitive tilt sensor with strain-chirped fiber Bragg gratings," *IEEE Photon. Technol. Lett.*, vol. 17, no. 11, pp. 2394–2396, Nov. 2005, doi: 10.1109/LPT.2005.857978.

[43] A. P. Bazakutsa, O. V. Butov, and K. M. Golant, "Influence of hydrogen loading on active fibers," in *Proc. Opt. Fiber Commun. Conf./National Fiber Optic Eng. Conf.*, May 2014, pp. 2–5, doi: 10.1364/nfoec.2013.jth2a.20.

[44] H. Lee, R.-I. Eom, and Y. Lee, "Evaluation of the mechanical properties of porous thermoplastic polyurethane obtained by 3D printing for protective gear," *Adv. Mater. Sci. Eng.*, vol. 2019, pp. 1–10, Dec. 2019, doi: 10.1155/2019/5838361.

[45] V. C. Pinto et al., "Comparative failure analysis of PLA, PLA/GNP and PLA/CNT-COOH biodegradable nanocomposites thin films," *Proc. Eng.*, vol. 114, pp. 635–642, Jan. 2015, doi: 10.1016/j.proeng.2015.08.004.

M. S. M. Sa'ad received the Bachelor of Science (Hons.) degree in pure physics from the Faculty of Science, University of Malaya, Kuala Lumpur, Malaysia, in 2018, where he is currently the master's degree.

He is a Research Assistant at the Photonics Research Center, University of Malaya. His research interests include fiber optic sensors mainly on fiber Bragg gratings.

H. Ahmad received the Ph.D. degree in laser technology from the University of Wales, Swansea, U.K., in 1983.

He is currently a Professor with the Department of Physics and the Director of the Photonics Research Center, University of Malaya, Kuala Lumpur, Malaysia, where he has actively pursued research activities in the field of photonics since 1983. He is the author of more than 400 professional papers in international journals and conference proceedings. His research interests are in lasers, fiber-based devices for telecommunications, and fiber-based sensor devices.

Dr. Ahmad is a Fellow of the Academy of Sciences, Malaysia.

M. A. Alias received the Bachelor of Science (Hons.) degree in industrial physics from the Faculty of Science, Universiti Teknologi Malaysia (UTM), Kuala Lumpur, Malaysia, in 2020. He is currently pursuing the master's degree with the Photonics Research Center, University of Malaya.

He is a Research Assistant at the Photonics Research Center, University of Malaya. His current research interests include optical fiber sensors mainly on fiber Bragg gratings.

M. K. A. Zaini received the bachelor's degree from the Department of Physics, Faculty of Science, University Putra Malaysia, Seri Kembangan, Malaysia, in 2015. He is currently pursuing the master's degree with the Photonics Research Center, University of Malaya, Kuala Lumpur, Malaysia.

His current research interests include fiber Bragg grating sensors and spatial division multiplexing.

K. S. Lim (Senior Member, IEEE) received the B.E. degree from the Department of Electrical Engineering, Faculty of Engineering, University of Malaya, Kuala Lumpur, Malaysia, in 2008, and the Ph.D. degree from the Photonics Research Center, Department of Physics, University of Malaya, in 2012.

He is currently a Senior Lecturer with the Photonics Research Center, University of Malaya. His current research interests include fiber Bragg grating sensors, spatial division multiplexing, and laser medical devices.

Dr. Lim is a Corporate Member of the Institute of Engineers Malaysia (IEM), a registered Professional Engineer (Telecommunication) of the Board of Engineers Malaysia (BEM), and a member of OSA.

S. W. Harun received the bachelor's degree in electrical and electronics system engineering from the Nagaoka University of Technology, Nagaoka, Japan, in 1996, and the master's and Ph.D. degrees in photonics technology from the University of Malaya, Kuala Lumpur, Malaysia, in 2001 and 2004, respectively.

He has more than 20 years of research experience in the development of optical fiber devices including fiber amplifiers, fiber lasers, and fiber optic sensors. He has published more than 900 articles in reputable ISI journals, and his papers have been cited more than 8000 times with an H-index of more than 40, showing the impact on the community.

Dr. Harun is a Fellow of the Malaysian Academic of Science and the Founder and an Honorary Advisor for the Optical Society of Malaysia.

K. T. V. Grattan received the B.Sc. (Hons.) degree in physics and the Ph.D. degree in laser physics from Queen's University Belfast, Belfast, U.K., in 1974 and 1979, respectively, and the D.Sc. degree from City University, London, U.K., in 1992, for his sensor work. His doctoral research involved the use of laser-probe techniques for measurements on potential new laser systems.

His research interests have expanded to include the development and use of fiber optic and optical systems in the measurement of a range of physical and chemical parameters.

B. M. A. Rahman (Life Fellow, IEEE) received the B.Sc.Eng. and M.Sc.Eng. (Hons.) degrees in electrical engineering from the Bangladesh University of Engineering and Technology (BUET), Dhaka, Bangladesh, in 1976 and 1979, respectively, and the Ph.D. degree in electronic engineering from University College London, London, U.K., in 1982.

From 1976 to 1979, he was a Lecturer at the Electrical Engineering Department, BUET. In 1988, he joined the Electrical, Electronic and Information Engineering Department, City University, London, as a Lecturer, where he is now a Professor. At City University, he leads the Research Group on Photonics Modeling, specialized in the development and use of the rigorous and full-vectorial numerical approaches, frequency-domain modal solution approach, the beam propagation method, and time-domain approach, primarily based on the numerically efficient finite-element method.

G. Brambilla received the M.Sc. (Hons.) degree in engineering from the Politecnico di Milano, Milan, Italy, in 1996, and the Ph.D. degree in optoelectronics from the University of Southampton, Southampton, U.K., in 2002.

Since 2016, he has been the Co-Director and the General Manager of the Future Photonics Hub. He has been the Director of the Centre for Innovative Manufacturing in Photonics until 2015. He is a Professor at the Optoelectronics Research Centre. His research interests include optical fiber sensors, optical fiber structuring using fs lasers, specialty and polymer fibers, new fiber fabrication technologies, UV fiber lasers, devices based on optical fiber nanowires, fiber tapers and couplers, rare-earth-doped scintillating fibers, and fibers for nuclear sensing.

Dr. Brambilla was awarded the Royal Society Research Fellowship in 2007, which was then extended in 2012.

S. A. Reduan received the Bachelor of Science (Hons.) degree in physics from the Faculty of Science, Universiti Teknologi Malaysia (UTM), Johor, Malaysia, in 2015, and the Ph.D. degree from Universiti Malaya, Kuala Lumpur, Malaysia, in 2020.

Her research interests include pulsed laser, saturable absorber, and fluoride fiber-based laser.

L. Bayang received the B.Eng. and M.Eng. degrees from the University of Malaya, Kuala Lumpur, Malaysia, in 2006 and 2015, respectively.

He is currently a Research Officer with the Photonic Research Centre, University of Malaya. He has coauthored numerous ISI professional articles and presented his work in many conferences. His current research interests include equipment test and measurement and the development of fast and ultrafast fiber lasers.

M. F. Ismail received the Bachelor of Engineering degree in telecommunication and the Master of Engineering degree in science from the Faculty of Engineering, University of Malaya, Kuala Lumpur, Malaysia, in 1999 and 2004, respectively.

His research interests include pulsed, multi-wavelength fiber lasers, and waveguides.